A review of the synthesis, characterization, and mechanism of bimetallic catalysts for electrocatalytic CO_2 reduction

LIAO Yin-li[1], HUANG Heng-bo[2], ZOU Ru-yu[1], SHEN Shu-ling[1], LIU Xin-juan[1], TANG Zhi-hong[1,*]

（1. *School of Materials and Chemistry*, *University of Shanghai for Science and Technology*, *Shanghai* 200093, *China*;
2. *Shanghai Shengsheng Chemical Technology Co.*, *Ltd*, *Shanghai* 200082, *China*）

Abstract: The electrocatalytic CO_2 reduction reaction (CO_2RR) is an environmentally friendly way to convert CO_2 into valuable chemicals. However, CO_2 conversion is a complex process, which contains 2, 4, 6, 8, and 12 electron transfer processes. It is very important to develop efficient catalysts to precisely control the number of electron transfers for the chemicals required. Single-metal catalysts have some deficiencies, including slow reaction kinetics, low product selectivity and inadequate stability. In response to these challenges, bimetallic catalysts have received significant attention owing to their unique structure and improved performance. The introduction of secondary metals alters the catalyst's electronic structure, and creates novel active sites, as well as optimizing their interaction with the intermediates. This review provides a comprehensive account of atomically distributed bimetals based on carbon materials and non-atomic distributed bimetals such as alloys and heterostructures, including their synthesis methods, characterization, and the outcomes of different catalysts. Catalytic mechanisms of different bimetallic catalysts are proposed and challenges encountered in the CO_2RR are considered.

Key words: CO_2 reduction reaction; Bimetallic catalysts; Synergistic effect; Electrocatalysts

1 Introduction

Carbon dioxide emissions resulting from the overconsumption of fossil fuels have led to serious climate hazards, the overarching effects of which are often irreversible within 1 000 years[1,2]. As a result, it is imperative to either reduce CO_2 emissions or convert it to valuable chemicals. The electroreduction of CO_2 is an effective and clean strategy for CO_2 reduction[3–5]. CO_2 reduction involves a variety of reaction paths (Table 1). Commonly there are 2, 4, 6, 8 and 12 electron transfer processes[6–8]. The resulting products, such as CO and syngas ($CO+H_2$), can be used to produce hydrocarbons or oxygenates by the Fischer-Tropsch synthesis method[9,10], and other chemicals such as methanol, formaldehyde, methane, ethanol, and several others can also be obtained from CO_2 reduction. The products of CO_2 reduction are sensitive to the practical applications and tends to produce a variety of products, which is one of the significant challenges in this area. On the other hand, considerable thermodynamic and kinetic barriers caused by the stable C＝O bond exist in the process of CO_2 reduction[11–13]. Additionally, a competing hydrogen evolution reaction (HER) is also unavoidable[14–16]. Therefore, it is of great significance to develop efficient catalysts to improve CO_2 reduction reaction (CO_2RR)[17,18].

Single-atom catalysts (SACs) have attracted significant attention in the field of CO_2RR due to their good catalytic performance. The unsaturated coordination configuration of atoms in SACs makes them more active in many reactions. In addition, SACs allow for the design of active sites with well-defined positions through the tunable coordination environment, resulting in excellent activity and selectivity for specific reactions[19–21]. For instance, Yang et al.[22] designed a catalyst containing high dispersions of $Fe-N_4$ moieties with a hierarchical structure, which prevented the migration and aggregation of Fe^{3+} due to the strong binding between metal ions and nitrogen. The porous structure of the catalyst also facilitated fast ion transfer and allowed for sufficient exposure of active

Received date: 2024-01-28; **Revised date:** 2024-04-30

Corresponding author: TANG Zhi-hong, Associate Professor. E-mail: zhtang@usst.edu.cn

Author introduction: LIAO Yin-li, Master Student. E-mail: liaoyinli2021@163.com

Table 1 The standard potentials of CO_2RR at ambient conditions

Transferred electron number	Half electrochemical thermodynamic reactions	E°/V(vs. SHE)
$1e^-$	$CO_2 + e^- \rightarrow CO_2^-$	−1.90
	$CO_2 + 2H^+ + 2e^- \rightarrow CO + H_2O$	−0.53
$2e^-$	$2CO_2 + 2H^+ + 2e^- \rightarrow HCOOH$	−0.61
	$2CO_2 + 2H^+ + 2e^- \rightarrow H_2C_2O_4$	−0.91
$4e^-$	$CO_2 + 4H^+ + 4e^- \rightarrow HCHO + H_2O$	−0.48
$6e^-$	$CO_2 + 6H^+ + 6e^- \rightarrow CH_3OH + H_2O$	−0.38
$8e^-$	$CO_2 + 8H^+ + 8e^- \rightarrow CH_4 + 2H_2O$	−0.24
$12e^-$	$2CO_2 + 12H^+ + 12e^- \rightarrow C_2H_4 + 4H_2O$	−0.35
	$2CO_2 + 12H^+ + 12e^- \rightarrow C_2H_5OH + 3H_2O$	−0.33
$14e^-$	$2CO_2 + 14H^+ + 14e^- \rightarrow C_2H_6 + 4H_2O$	−0.27
$18e^-$	$3CO_2 + 18H^+ + 18e^- \rightarrow C_3H_7OH + 3H_2O$	−0.31

sites, ultimately improving the selectivity of the catalyst. The Faraday efficiency of CO (FE_{CO}) achieved by this catalyst was up to 89%. However, SAC has only one active site and faces challenges in breaking the linear proportional relationship between intermediates when more complex reactions are conducted[23].

Recent researches have shown that the synergistic effect between adjacent atoms in bimetallic catalysts can significantly improve catalytic performance compared to isolated atoms. First, the introduction of secondary metals can alter the electronic structure of catalyst surface, thereby optimizing the adsorption and desorption of intermediates, and ultimately improving catalytic efficiency[24,25]. For example, Gao et al. prepared In-Ga metal-organic-frameworks with abundant In-Ga bimetallic sites (InGa MOFs)[26]. The atomic bridging between Ga and In atoms effectively optimized the electronic structure of In, weakening In-C hybridization and enhancing In-O hybridization. This modification reduced the adsorption of the key intermediate *COOH involved in the competitive CO pathway, while enhancing the adsorption of *OCHO (formate pathway), in the end, promoting CO_2 reduction to formate. Additionally, single metal catalysts offer only one active site, restricting CO_2RR to occur on a single position and fixing the adsorption energy of intermediates. In contrast, bimetallic catalysts offer multiple types of adsorption sites, divide the reaction path into several segments, and break the linear proportional relationship of intermediates. For instance, crucial intermediates like *COOH, *CHO and *CO in the CO_2RR process can be adsorbed on different active sites[27]. The tandem catalysis occurs on bimetallic catalysts by utilizing adjacent adsorption sites, increasing the reaction rate and leading to the production of high-value C_{2+} products. Chen et al.[28] synthesized a CoPc@HC/Cu bimetallic catalyst, which decomposed CO_2 to C_{2+} through 2 distinct reactions: CO_2 to CO and CO to C_{2+}. The CoPc@HC exhibited high selectivity on the reduction of CO_2 to CO, elevated the local CO concentration, and enhanced the C—C coupling reaction on Cu. Thus, bimetallic catalysts provide a more complex and flexible material selection opportunity, enabling the design of different active centers according to the desired outcomes[29].

The research of bimetallic catalysts is a hot topic in CO_2RR due to their excellent electrocatalytic activity and long-term stability. This paper proposes a brief review of recent progress in the development of bimetallic catalysts for CO_2RR. The types of bimetallic catalysts, synthesis methods, characterization and outcomes are comprehensively summarized, the structure-active site relationship and the synergistic effect between metals in bimetallic catalysts are mainly focused. Finally, the future challenges and development prospects are put forward, and the potential for further research in this area is highlighted (Fig. 1).

2 Types of bimetallic catalysts

Bimetallic catalysts can be classified into 2 types based on the distribution of metal atoms: Atomic and non-atomic distributions.

The atomic-level distribution refers to double-atom catalysts (DACs) composed of MN_x-$M'N_x$ moieties, where M and M' represent metal atoms. The catalytic activity of DACs is mainly attributed to the synergy between adjacent metal atoms, which is enhanced by introducing sub-metals that alter the electronic configuration of the active site. DACs can be homonuclear where M and M' are the same, or heteronuclear[30]. Homonuclear DACs provide symmetric adsorption sites for reactant molecules, which are usually more thermodynamically stable than single-atom

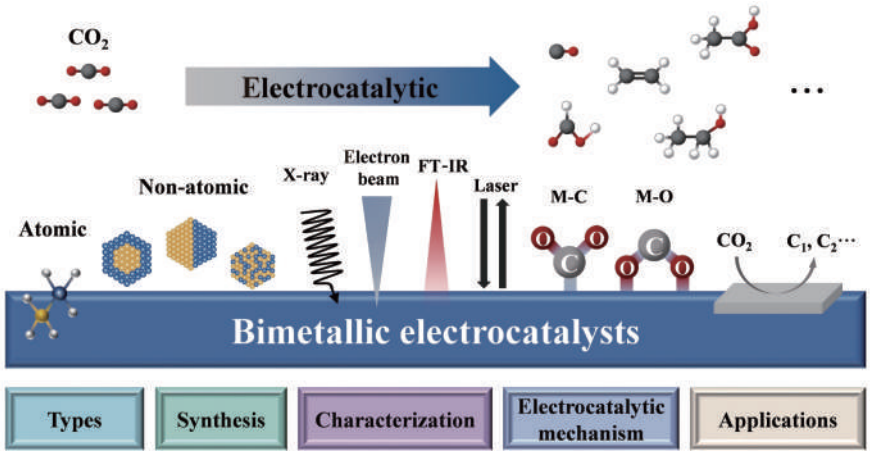

Fig. 1　Overview on the categories of bimetallic electrocatalysts

catalysts due to the lower free energy of metal dimers. For instance, Wang et al.[31] successfully synthesized homonuclear DACs with a unique Fe_2-N_6 configuration by anchoring Fe_2 atoms atomically dispersed on N-doped carbon substrates (Fig. 2a, b). This catalyst exhibited superior intrinsic activity, CO selectivity and stability compared to single-atom Fe_1-N_x-C. Heteronuclear catalysts compose 2 or more different types of metal atoms, offering a unique opportunity to adjust the electronic structure of active sites through bimetallic interactions. This electronic structure regulation optimizes intermediate adsorption, reduces reaction barriers and refines pathways, ultimately improving catalytic activity. Wang et al.[32] synthesized CuFe/N—C heteronuclear catalysts by anchoring Fe and Cu on N-doped carbon frameworks. Here, Fe acted as the adsorption site for the intermediate, and the addition of Cu enhanced the adsorption of the intermediate *COOH, promoting the CO_2RR. Furthermore, bimetallic atoms can serve as adsorption sites for different types of atoms. Density functional theory calculations showed that the 2 metal atoms acted as carbon adsorption site and oxygen adsorption site in CuCr/C_2N and CuMn/C_2N, respectively[24]. This enhanced their binding with *COOH or *CHO intermediates while having negligible effect on the binding of *CO, achieving efficient reduction of CO_2 to CH_4. Atomic distribution is efficient to improve the utilization efficiency of metal atoms. However, metal monomers are prone to aggregate, so diatomic sites must be firmly anchored on the substrate. Porous substrates can be constructed to anchor metal atoms[33]. Carbon materials have good conductivity, high surface area, excellent thermal and chemical stability, making them an excellent substrate for anchoring metal atoms after defect design. A larger specific surface area increases the number of exposed active sites. Single atoms Ni and Ag were anchored onto defective nitrogen-rich porous carbon through cascading pyrolysis, and metal atoms were stabilized in the catalyst through N bonding with the substrate[34]. Double atom site Ni-Ag reduced the adsorption capacity of Ni atoms for *CO through the introduction of Ag atoms, and lowered the energy barrier for the formation of *COOH intermediates on the surface. Compared to catalysts with adjacent bimetallic atoms, those with randomly dispersed atoms are easier to prepare. Josh Leverett et al.[35] prepared bimetallic catalysts featuring unsaturated coordination of Ni-N_x and Fe-N_x on holey graphene (Ni-hG/Fe-hG) (Fig. 2c). Uniformly distributed Ni and Fe atoms were observed by high-angle annular dark-field scanning transmission electron microscope (HAADF-TEM) (Fig. 2d). By adjusting the ratio of Ni-hG and Fe-hG, the researchers were able to achieve syngas with a wide range of CO to H_2 ratio. This spanned between the values obtained from pure Ni-hG (with FECO > 90%) and pure Fe-hG (with FEH_2 > 90%).

Non-atomic distribution bimetallic catalysts, formed by core-shell structures or alloys, enable tandem catalysis[36]. Initially, a relatively simple CO_2RR occurs on one metal atom, such as the formation of in-

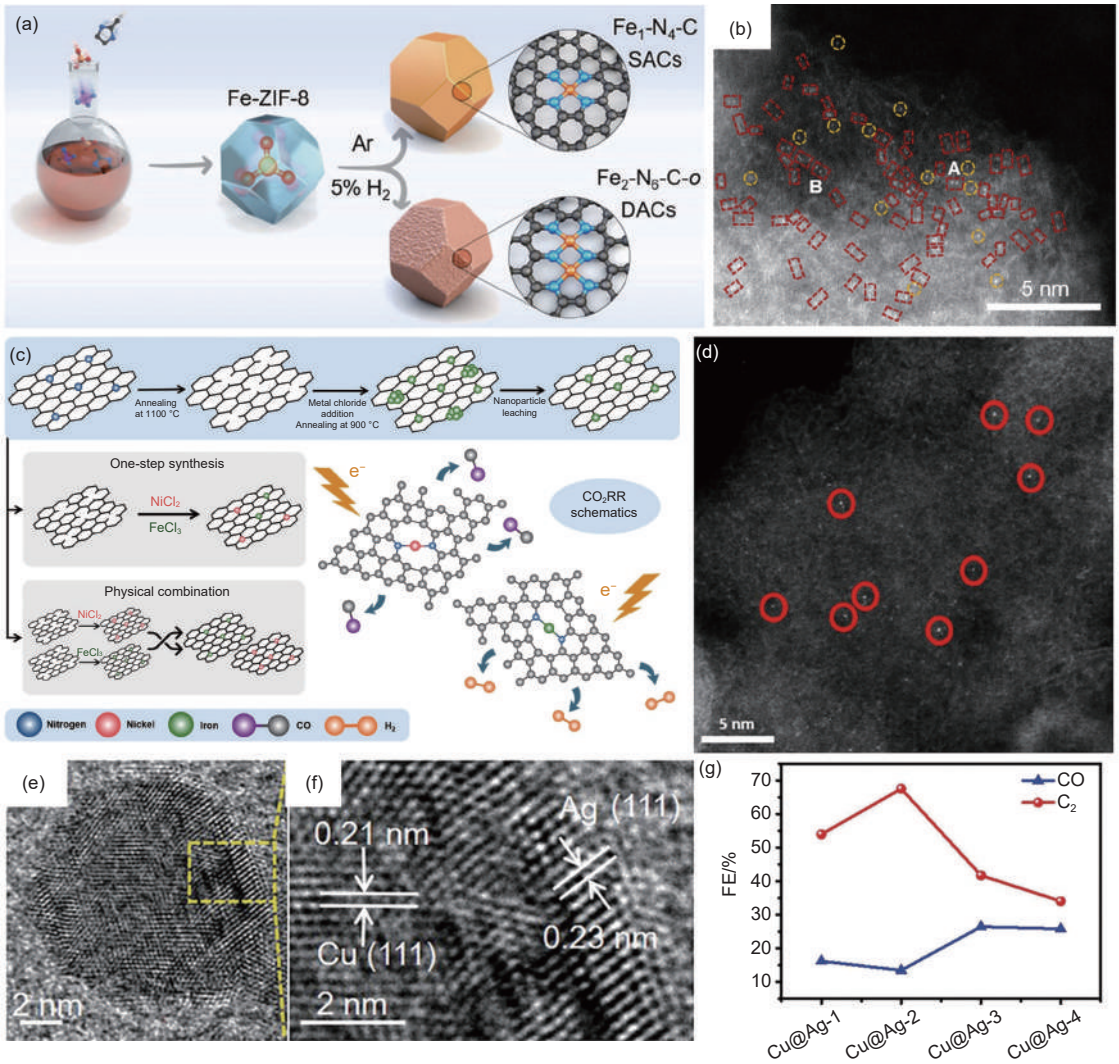

Fig. 2 (a) Schematic of the preparation process of Fe_1-N_4-C and Fe_2-N_6-C-o. Reproduced by permission of American Chemical Society[31]. (b) The aberration-corrected high-angle annular dark field scanning transmission electron microscopy (AC-HAADF-STEM) image of Fe_2-N_6-C-o. Reproduced by permission of American Chemical Society[31]. (c) Schematics representing the synthesis method used to prepare undercoordinated Ni-N_x and Fe-N_x active sites. Reproduced by permission of American Chemical Society[35]. (d) HAADF-STEM images for one-step synthesized Ni, Fe-hG. Reproduced by permission of American Chemical Society[35]. (e, f) High-resolution TEM (HRTEM) images of Cu@Ag-2. Reproduced by permission of Wiley-VCH[40]. (g) FEs of CO and C_2 for the Cu@Ag. Reproduced by permission of Wiley-VCH[40]

termediate *CO. After desorption, a large number of intermediates gather nearby and then adsorb on another metal atom to catalyze more complex reactions, resulting in a C_{2+} product[37]. Commonly, CO_2RR is a complex reaction and there is a competitive reaction of HER, which creates a bottleneck for complex reduction reactions hindering the formation of more complex chemicals. Therefore, CO and formate are often obtained through a $2e^-$ reaction pathway. Tandem catalysis allows CO_2RR to enter more complex stages to synthesize more advanced hydrocarbons and oxygenates, thereby expanding the possibilities beyond the $2e^-$ reaction pathway. Copper-based catalysts have unique C—C coupling ability, which can convert CO_2 into C_{2+}. Tandem catalysis of Cu with other metals greatly promotes the selectivity of C_{2+}[38,39]. For instance, Zhang et al.[40] developed a Cu@Ag catalyst with a core-shell structure to generate large amounts of CO on the Ag shell (Fig. 2e, f). CO was diffused to the Cu core for C—C coupling, realizing the tandem catalysis of CO_2 conversion. The selectivity of C_2 was also improved, with the FEC_2 up to 67.6% (Fig. 2g).

Non-atomic distribution bimetallic catalysts can regulate the electronic configuration of active sites by constructing nanoscale heterogeneous interfaces or defect engineering, thereby optimizing the adsorption

of intermediates. Defect engineering is an effective strategy that can regulate the local catalytic environment and corresponding electronic structure around adjacent atoms, alter the local density of states curve of surface atoms, and fundamentally enhance the intrinsic activity of materials. For example, Yang et al.[41] generated abundant oxygen vacancies (O_V) by constructing lattice mismatched Bi_2O_3 and In_2O_3. Oxygen vacancies weakened the activation energy of CO_2 and accelerated the separation and migration of local charges. Although non-atomically distributed bimetallic catalysts are relatively easy to prepare and suitable for industrial production (especially those composed of precious metals), their application is often hindered by challenges such as poor long-term stability and delayed kinetics in the complex chemical environments of industrial processes.

A common challenge faced by bimetallic catalysts is the agglomeration of the bimetallic atoms and the difficulty in precisely controlling their sites. Therefore, achieving precise control of the active sites during the synthesis process is critical. In the following section, we will introduce the commonly used methods for synthesizing bimetallic catalysts developed in recent years.

3 Synthesis of bimetallic catalysts

According to recent research, the synthesis of bimetallic catalyst can be classified into top-down and bottom-up strategies. Pyrolysis is the main top-down approach, which is generally used to prepare bimetallic catalysts with atomically dispersed MN_x-M'N_x moieties. Conversely, there are more bottom-up methods, such as wet chemical synthesis (WCS), electrochemical deposition (ECD), atomic layer deposition (ALD), and chemical vapor deposition (CVD), etc. These methods pose a challenge in accurately controlling the position of metal atoms and are mainly used to prepare bimetallic catalysts with non-atomic distribution. Further details on these 2 methods will be discussed in the following sections.

3.1 The top-down method for bimetallic catalysts

Since the surface free energy of metal atoms is high, preventing the agglomeration of metal atoms is a challenge during the synthesis and catalytic reactions of bimetallic catalysts. Therefore, it is essential to form covalent bond between the metal dimer and the coordinating atoms and then confine metal atoms through covalent bonds[42]. Pyrolysis using metal organic frameworks (MOF)/zeolite imidazole ester frameworks (ZIF) as sacrificial templates can effectively solve the problem of atomic dispersion. The bimetallic atoms are fixed onto these templates by containing specific metal atoms, which are then anchored onto carbon-based materials through thermal decomposition.

Chen et al.[44] reported the synthesis of Ni/Cu-N-C catalysts with adjacent N_xNi/CuN_x groups loaded on an N-rich carbon substrate by pyrolysis of zeolitic imidazolate framework-8(ZIF-8). The synthesis process of Ni/Cu is schematically outlined in Fig. 3a. In this process, ZIF-8 acted as a molecular cage, trapping $Ni(acac)_2$ in its cavity. The material in the cavity could further accelerate the decomposition of the connections between the metal atoms and the imidazolium salt, expanding the voids inside. A one-step thermal activation removed Zn atoms and doped Cu atoms. Finally, Cu was coordinated with N, and Ni/Cu—N—C catalyst with atomic dispersion was obtained. The electronic reconstruction of Ni induced by adjacent CuN_4 sites enhanced the adsorption of *COOH, facilitating the production of CO. The catalyst with the N_4Ni/CuN_4 group exhibited excellent catalytic activity and selectivity, achieving a maximum FE_{CO} of 99.2% at −0.79 V *vs*. RHE. Another example of top-down synthesis was the synthesis of Ni/Fe—N—C catalysts[45]. Firstly, iron (Fe) ions were chemically bonded to organic ligands, serving as nodes, achieving atomic-level dispersion of Fe without agglomeration. Subsequently, nickel nitrate was encapsulated within the ZIF-8 framework using a dual solvent approach. Finally, the Zn material was removed by pyrolysis, resulting in the production of atomically dispersed Ni/Fe—N—C diatomic catalysts. Scanning transmission electron microscopy (STEM) and X-ray absorption spectroscopy (XAS) revealed the formation of diatomic sites. The synergistic effect

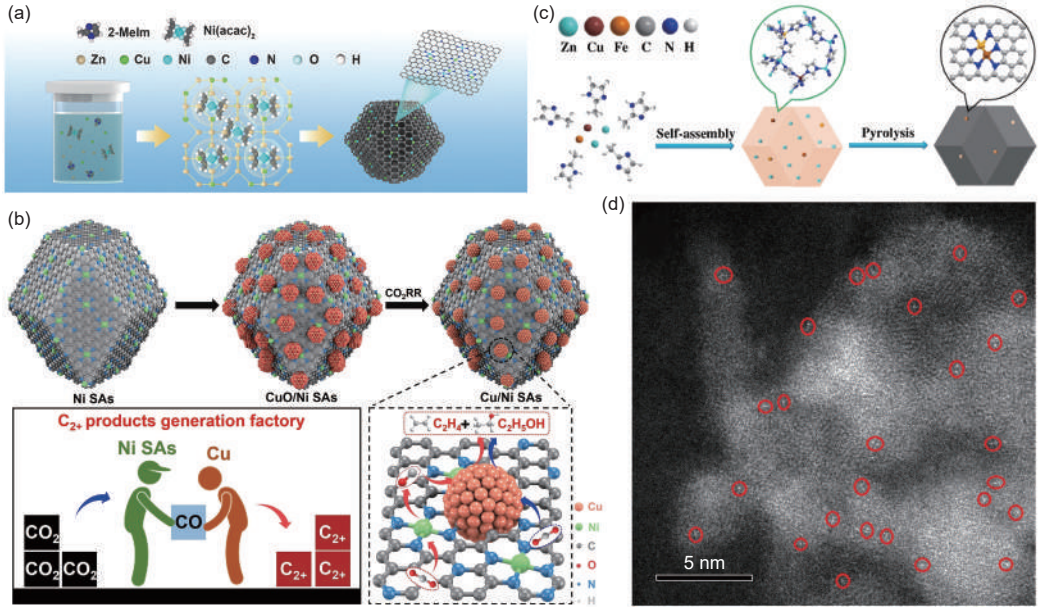

Fig. 3 (a) Synthesis schematic of Ni/Cu—N—C. Reproduced by permission of American Chemical Society[44]. (b) The schematic diagram of the synthesis mechanism of CuO/Ni SAs tandem catalyst. Reproduced by permission of Elsevier[46]. (c) Scheme for the synthesis of CuFe/N—C. Reproduced by permission of Elsevier[32]. (d) Magnified HAADF-STEM image of CuFe/N—C. Reproduced by permission of Elsevier[32]

of neighboring Ni and Fe reduced the reaction barrier for *COOH formation and CO desorption, improving the selectivity of CO. Zhang et al.[46] prepared atomic-dispersed CuO/Ni single atoms (SAs) tandem catalysts using a pyrolysis method (Fig. 3b). Initially, they achieved the uniform dispersion of Ni SAs by taking advantage of the uniform coordination environment provided by ZIF-8 and the high-density nitrogen doping defects. Subsequently, CuO was loaded onto the catalyst, forming a close bond with Ni SAs/N—C. The high dispersion of Ni SAs and the short distance between bimetallic active sites not only enhanced the efficiency of CO intermediate utilization, but also mitigated the impact of CO mass transfer on the rate of C_{2+} product generation. Similarly, Wang et al.[32] prepared CuFe/N—C catalysts with atomic dispersion by the pyrolysis method and the position of the bimetallic atom could be observed by the HAADF-STEM image (Fig. 3c, d). However, excessive dopant metals tend to aggregate, and the precise control of many parameters for bimetals is required, making their large scale production challenging.

3.2 The bottom-up method for bimetallic catalysts

Compared to top-down strategies, bottom-up strategies are more repeatable. In this strategy, mono- or polynuclear metal complexes are firstly fixed on the support, and then the metal precursors are reduced and confined in vacancies under high-temperature pyrolysis[43]. The random location of metal introduction and weak interaction between metal and substrate are the two problems of this method.

There are several bottom-up methods for preparing bimetallic catalysts, with the wet chemical method being a popular and relatively simple one. This method is generally low cost and enables the synthesis of well dispersed metal atoms or metal clusters. Typically, the preparation process involves 3 steps: (1) introducing the metal precursor onto the carrier via impregnation/ion exchange, coprecipitation, or deposition-precipitation under suitable pH conditions; (2) drying the resulting mixture; (3) reducing the metal through calcination to enhance the interaction between the metal and carrier and prevent metals from aggregation[47]. For instance, Gong et al.[48] used a wet chemical method to prepare Ni/Fe—N/O—C bimetallic catalysts with ultra-low metal loading capacity (Fig. 4a). Ni^{2+} and Fe^{3+} were captured and adsorbed onto N doped activated carbon black, followed by etching with HCl to enhance the interaction between

the metal and the substrate, resulting in the formation of a Ni/Fe N/O—C bimetallic catalyst. The activation of carbon black was a crucial step, increasing the degree of defects in the substrate and anchoring metal atoms through these defects. In addition, the spherical structure facilitated the diffusion of CO_2 and increased the concentration of local reactants on the electrode surface. The introduction of secondary metal regulated the electronic structure of the active center, thereby synergistically reducing the energy barrier formed by *COOH. Similarly, Zhang et al.[49] prepared a ZnO-Ag bimetallic catalyst from activated carbon spheres with an ultra-high surface area. Firstly, zinc nitrate and silver nitrate were dispersed in the pores of the activated carbon spheres via wet impregnation. Then, ZnO-Ag@UC with the "two ships in a bottle" structure was obtained by pyrolysis (Fig. 4b). High-resolution transmission electron microscopy (HRTEM) images revealed that heterointerfaces were formed between Ag and ZnO (Fig. 4c). Electron delocalization from Zn and Ag to O not only improved CO selectivity by stabilizing *COOH but also inhibited formate and H_2 production. In addition, HAADF-STEM image showed that the ZnO-Ag nanoparticles were uniformly distributed in the activated carbon spheres (Fig. 4d), indicating that the "two ships in a bottle" structure could achieve the uniform dispersibility of bimetallic atoms, which could be applied to preparing other bimetallic catalysts. In these examples, an active surface area is an important factor improving the catalytic performance. The construction of defects provided anchoring points for metal atoms, and then stabilized and prevented them from aggregation. The wet chemical method is a versatile technique for preparing various types of bimetallic catalysts. Due to its wide applicability and straightforward procedure, the wet chemical method has emerged as one of the most promising approaches for industrial catalyst production.

Electrochemical deposition is another efficient bottom-up method used for the preparation of bimetallic catalysts. This process involves the addition of target metal-containing compounds to the electrolyte, followed by the reduction and deposition of the metal onto the working electrode. The electrochemical deposition process often accompanies HER, and the hydrogen obtained can often be used as the soft template to prepare advanced catalysts. For instance, Zeng et al.[50] fabricated Sn-modified porous Cu foam (Cu-Sn foam) with a three-dimensional porous dendrite core-shell structure through two-step electrochemical depositions, the SEM images of the obtained

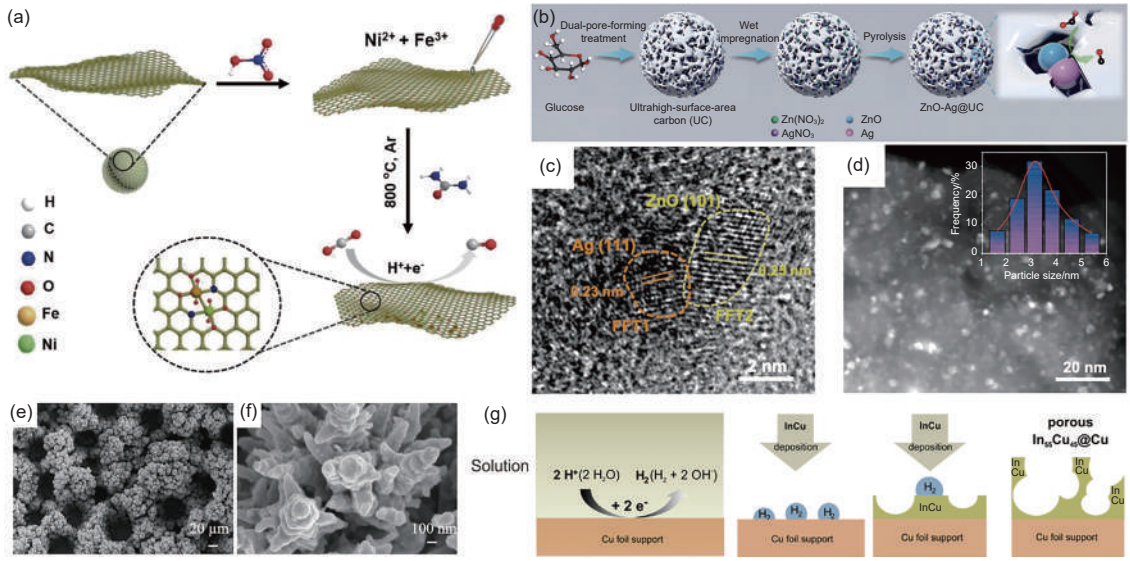

Fig. 4　(a) Synthesis schematic of Ni/Fe-N/O-C. Reproduced by permission of Wiley-VCH[48]. (b) Schematic of the synthesis route of ZnO-Ag@UC. Reproduced by permission of American Chemical Society[49]. (c) HRTEM image and (d) HAADF-STEM image of ZnO-Ag@UC. Reproduced by permission of American Chemical Society[49]. (e, f) SEM images of Cu-Sn foams. Reproduced by permission of Elsevier[50]. (g) Schematic diagram of dynamic hydrogen bubble template (DHBT) method. Reproduced by permission of American Chemical Society[51]

sample are shown in Fig. 4(e, f). During the electrodeposition process, HER occurs under the applied current, leading to the formation of H_2 bubbles on the electrode surface, which acts as the template for electrodeposition. The random nucleation, growth, and detachment of H_2 bubbles during the process create a porous foam structure. The resulting catalyst has a high active surface area, which improves the CO_2RR catalytic performance. The Sn modified Cu foam reduced the adsorption of H and significantly inhibited HER. A dendritic porous $In_{55}Cu_{45}$@Cu catalyst was also synthesized by a similar method[51]. In was deposited onto Cu foils by electrochemical deposition and foam-structured catalysts were created using the dynamic hydrogen bubble template (DHBT) method, as illustrated in Fig. 4g. The introduction of In significantly reduced the M—CO binding strength and diminished the C—C coupling effect of Cu. The Faraday efficiency and partial current density of $In_{55}Cu_{45}$@Cu catalyst were basically unchanged during the long-term CO_2 electrolysis process. The catalyst's long-term stability was attributed to its low hydrogen formation rate.

The electrodeposition method for directly depositing the second metal onto the substrate is simple, easy to operate, and offers high repeatability. It can also be scaled up for large-scale preparation. Additionally, this method allows for the direct use of the resulting material as a self-supporting electrode, not only overcoming issues such as active sites being covered by binders but also exposing a larger electrochemical active surface area. However, successful electrodeposition largely depends on the selection of an appropriate electrolyte that can effectively deposit the metal ions onto the working electrode under applied current. Therefore, careful consideration and optimization of the electrolyte are critical for achieving a successful electrodeposition process.

A well-defined catalyst structure is crucial for understanding the relationship between the synthesis process, catalyst structure, active sites, and catalytic performance. This understanding can help in the design of highly efficient catalysts according to the desired catalytic performance. Advanced characterization techniques are essential for in-depth research.

4 Structure characterization of bimetallic catalysts

Although bimetallic catalysts for CO_2RR exhibit excellent catalytic performance, it is difficult to determine the fundamental reason for the improvement due to their diverse configurations. Thus, it is a great challenge to establish the relationship between structure and activity, advanced characterization techniques are necessary. In this section, advanced techniques for CO_2RR are introduced to analyze the structure and deduce the catalytic mechanism of bimetallic catalysts.

4.1 High-angle annular dark-field scanning transmission electron microscope

Transmission electron microscopy (TEM) is a technique used to observe the morphology and structure of catalysts. STEM is an incoherent imaging technology that shows imaging contrast[52,53]. HAADF-STEM is a widely used technology to observe single- and double-atom catalysts. It can reach atomic scale resolution and provide a clear view of the atomic structure of the catalyst[54]. The variations in brightness in HAADF-STEM images primarily result from differences in the atomic numbers (Z) of the elements.

For instance, when observing adjacent bimetal atoms with small Z differences, two adjacent bright spots are observed. However, if the Z difference is large, there will be 2 bright and dark spots. Fig. 5(a, b) shows the HAADF-STEM image of Ag_1-G and Ag_2-G catalysts[55]. In Fig. 5a, the uniformly distributed bright spots in the red circle represent Ag of the single atom, rather than C of the substrate material, the different brightness is due to the difference in Z values of the substrate and Ag. As shown in Fig. 5b, adjacent double bright spots were observed, representing adjacent Ag_2 diatomic sites. Since both bright spots are Ag, the brightness is the same. HAADF-STEM has also been used to characterize the Ni/Fe—N—C catalyst and it was found that there are evenly distributed adjacent bright spots, proving the formation of diat-

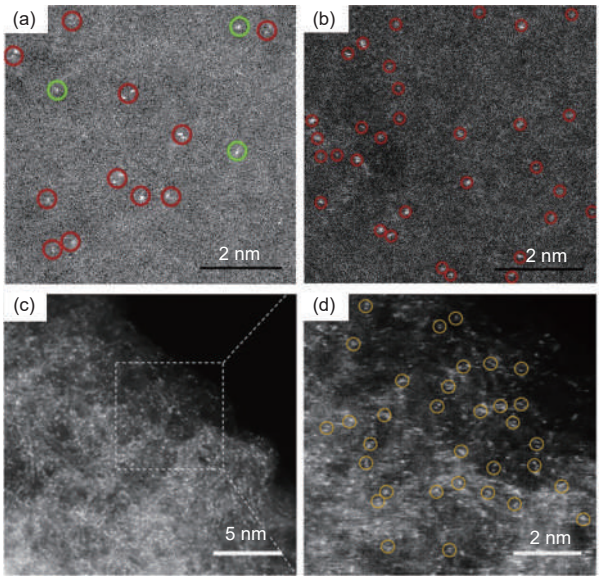

Fig. 5　Enlarged HAADF-STEM image of (a) Ag_1-G and (b)Ag_2-G. Reproduced by permission of Elsevier[55]. (c, d) Zoom-in HAADF-STEM images of Ni/Fe-N-C. Reproduced by permission of Wiley-VCH[45]

omic sites (Fig. 5c, d)[45]. By combining STEM and XAS, the generation of Ni-Fe sites was demonstrated, which was beneficial for reducing the energy barrier for the formation of intermediate *COOH and CO desorption. Advanced HAADF-STEM technique can provide atomic-level images, playing a crucial role in the characterization of bimetallic catalysts with atomic distribution.

4.2　X-ray absorption spectroscopy

XAS is a valuable technique for investigating the local characteristics of specific elements. It has been used to study the local environment of active sites and the interaction between metal and substrate[56,57]. Two major advancements in XAS are X-ray absorption near-edge structure (XANES) and extended X-ray absorption fine structure (EXAFS). These techniques are widely used to analyze the local chemical coordination environment of catalysts[58].

XANES is highly sensitive to the charge states of metals, adsorbates, and support materials, which can provide information on the electrons and local geometry around target atoms. As a result, XANES is an important tool for studying the electronic structure of catalytic materials[59]. EXAFS has high sensitivity to local structure and high spatial resolution, making it the preferred technology for studying the geometric properties of bimetallic catalysts[59–61]. These 2 techniques can provide complementary information for the same bimetallic catalyst and enable a comprehensive understanding of the system[62].

For example, Yang et al.[63] used XAS to explore the coordination environment of Fe and Co in the p-FeNC@CoNC catalyst. The Fe K-edge XANES spectrum of the catalyst, shown on the left of the reference FePc in Fig. 6a, suggested that the Fe atomic oxidation state was lower than that of FePc. Similarly, the Co K-edge XANES spectrum indicated that the Co oxidation state in p-FeNC@CoNC was approximately equal to that of CoPc (Fig. 6b). Furthermore, the EXAFS fitting revealed that there was no metal-metal bonding, but Fe—N and Co—N bonding appeared, indicating that Fe and Co might be separated at the atomic level (Fig. 6c, d). The model fitting based on EXAFS also showed that almost all Fe and Co in the samples were coordinated with four N atoms (Fig. 6e, f). XAS characterization confirmed that Fe and Co existed as single atoms in the catalyst and coordinated with 4 nitrogen atoms. The synergistic effect of the nuclear Co atom and the shell Fe atom promoted CO_2RR. Similarly, Hu et al.[64] used XANES and EXAFS to analyze the local structure of Cu in the a-CuTi@Cu catalyst before and after CO_2RR. The XANES spectra showed that the peak of a-CuTi@Cu was red-shifted compared with Cu foil, indicating that the introduction of Ti altered the electronic structure of Cu atoms (Fig. 6g). The low electronegativity of Ti enabled the transfer of electrons to Cu and increased the electron density of coordination unsaturated Cu sites, thereby promoting dimerization and trimerization of *CO intermediates. According to the EXAFS fitting results (Fig. 6h), the coordination number of Cu atoms on the catalyst surface was reduced after CO_2RR, indicating that many defects, such as vacancies, were generated. Combining the results of XANES and EXAFS, it can be concluded that the oxygen bonded with Ti and stabilized the Cu^I oxide. The valence band electrons of Cu^I sites participated in CO adsorption, which was beneficial for the dimerization of C—C coupling, improving the selectivity of

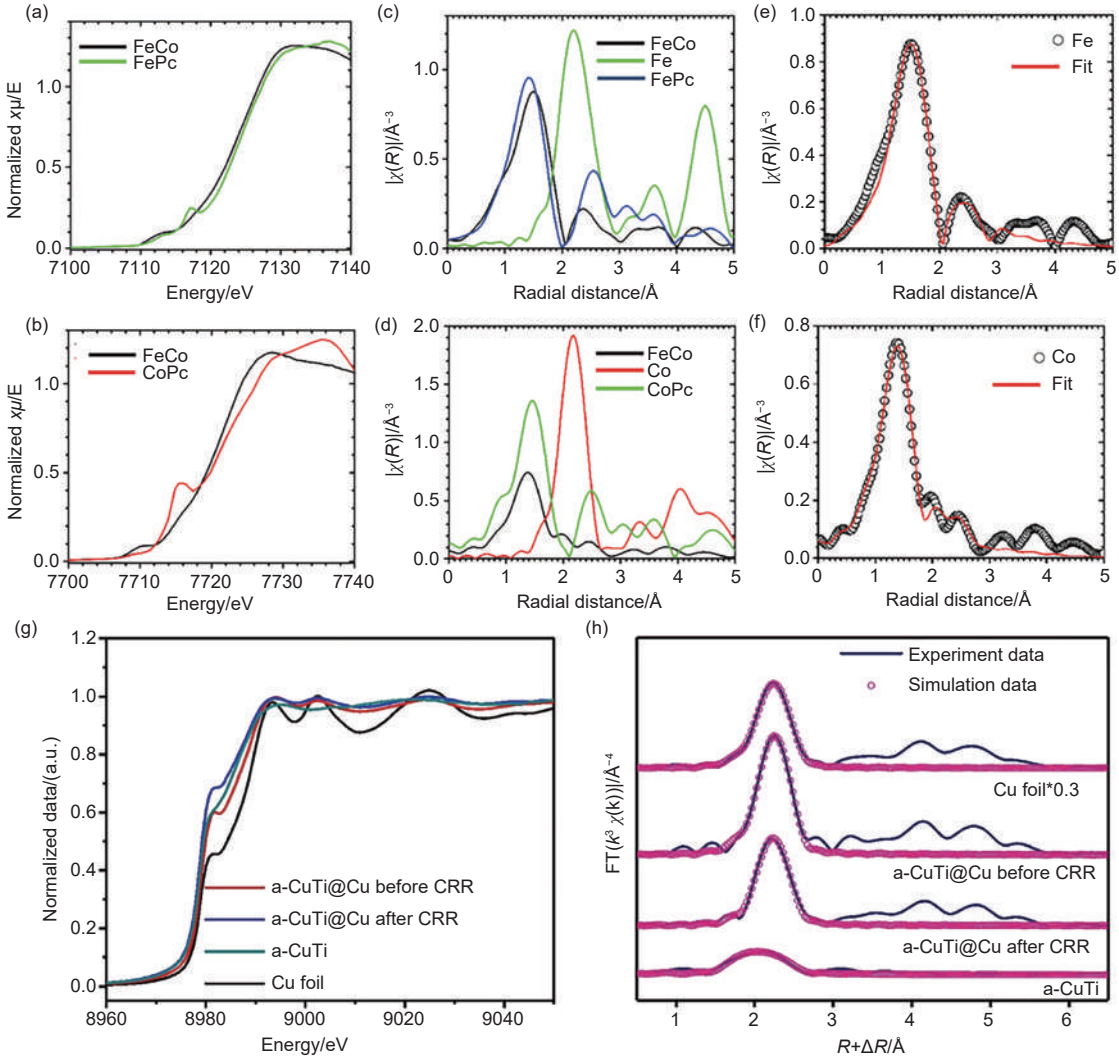

Fig. 6 (a, b) Fe and Co K-edge XANES spectra, (c, d) fit of the R-space EXAFS, and (e, f) Fourier-transform R-space fitting for the sample p-FeNC@CoNC (denoted as FeCo), respectively. Reproduced by permission of Wiley-VCH[63]. (g) XANES and (h) EXAFS spectra of a-CuTi@Cu before and after CO_2RR. Reproduced by permission of Wiley-VCH[64]

C_{2+} products. Researchers can get insights into the structure-activity relationship of the catalyst by using XAS to analyze the valence state change and coordination of an element in the catalyst.

4.3 In-situ/operando techniques for bimetallic catalysts

Although the role of each metal constituting the bimetallic catalysts can be investigated by many advanced characterizations, the reaction mechanism of the catalyst during CO_2RR is still not well understood. Therefore, in-situ/operando techniques are necessary. In particular, the roles of bimetallic catalysts during CO_2RR and how they act synergistically with each other require deeper investigations by employing in-situ/operando techniques.

Rahaman et al.[65] analyzed the in-situ changes of Pd_9Cu_{91} during CO_2RR using operando Raman spectroscopy. It was observed that the relevant characteristic peaks of cuprous oxide (518 and 624 cm^{-1}) had disappeared at 0 V (vs. RHE) (Fig. 7a), indicating that the oxides in the Pd_9Cu_{91} did not exist before the actual start of CO_2RR, reflecting the catalyst's instability during the reaction process. After electrochemical reduction, Cu_2O was reduced to metallic Cu in Pd_9Cu_{91}, and nanoscale rich Cu and Pd domains were formed in the catalyst. The Cu domain and Pd domain respectively served as producers of *CO and C—C coupling agents, thereby effectively improving reaction effi-

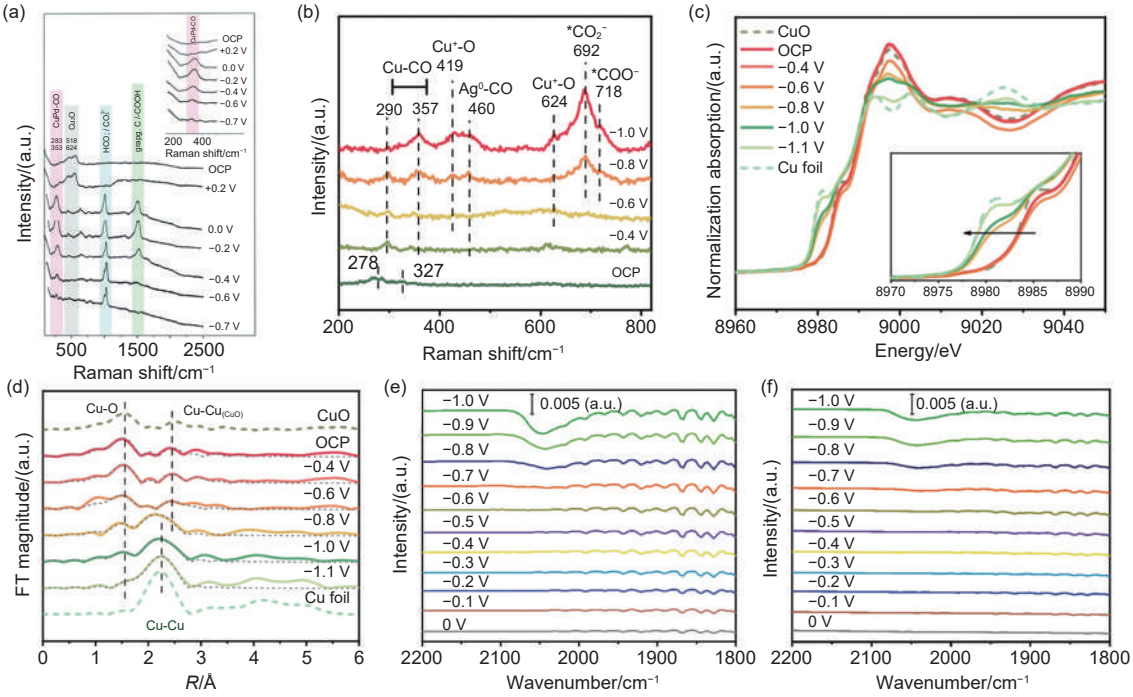

Fig. 7　(a) Potential-dependent operando Raman spectra of the od-Pd_9Cu_{91} foam sample. Reproduced by permission of Royal Society of Chemistry[65]. (b) In situ Raman spectroscopy of AgI-CuO catalysts. Reproduced by permission of Wiley-VCH[36]. (c) In-situ Cu K-edge XANES and corresponding first derivative XANES. Reproduced by permission of Wiley-VCH[36]. (d) In-situ Fourier-transform k^2-weighted EXAFS spectra of AgI-CuO catalysts. Reproduced by permission of Wiley-VCH[36]. In-situ ATR-IR spectra of (e) Au-Cu Janus NSs and (f) Cu nanoparticles. Reproduced by permission of Wiley-VCH[66]

ciency. Yang et al.[36] utilized in-situ Raman spectroscopy to investigate the structural evolution of AgI-CuO (Fig. 7b). With increasing negative potential, a characteristic peak related to CO adsorption on the Ag^0 surface appeared (460 cm^{-1}), indicating the reduction of Ag^+. And the peaks at 419 and 624 cm^{-1} suggested the existence of Cu_2O, indicating that copper was not completely reduced during CO_2RR. Additionally, in-situ XAFS was used to study the metal species changes of AgI-CuO. In-situ Cu K-edge XANES of the AgI-Cu showed that the absorption edge energy shifted towards lower energies as the potential decreased, indicating a decrease in the valence of the Cu (Fig. 7c). Meanwhile, in-situ Fourier transform k^2-weighted EXAFS spectrum of the AgI-Cu showed that two peaks related to Cu—O and Cu—Cu appeared at the beginning of the applied voltage (Fig. 7d). As the electrochemical potential decreased, the peak of Cu—Cu began to appear, indicating that the Cu in the catalyst changed from CuO to metallic Cu after the voltage was applied. Combined with in-situ Raman results, it was observed that the CuO in the catalyst was partially reduced to metallic Cu, forming a mixed Cu^0/Cu^+ site after the voltage was applied. The Cu^0/Cu^+ interface significantly reduced the energy barrier of C—C coupling, thus improving the selectivity of C_{2+} to CO_2RR.

In addition to in-situ changes of the catalyst itself during the reaction, the changes of the intermediates and their interactions with the active sites are also worth analyzing. Therefore, the adsorption of intermediates after applying potential can also be studied through in-situ/operando techniques. In-situ attenuated total reflection infrared spectroscopy (ATR-IR) was utilized to identify changes in reaction intermediates during CO_2RR of Au—Cu Janus NSs catalysts[66]. As depicted in Fig. 7(e, f), both Au—Cu Janus NSs and Cu nanoparticles displayed a stretching band near 2 050 cm^{-1}, indicating the presence of the linearly atop-bound CO intermediate (CO_{ad}), and the peak area in the CO_{ad} band representing the degree of CO coverage on the catalyst surface. The peak area of the CO_{ad} band of Au—Cu Janus NSs increased significantly compared to that of Cu nanoparticles, indicating that

the concentration of CO had increased. Additionally, the adsorption intensities of CO on Au—Cu Janus NSs and Cu nanoparticles were similar, suggesting that the introduction of Au had little effect on the CO adsorption intensity. The improved performance was due to the increased CO coverage on the catalyst surface after the introduction of Au, which, in turn, promoted C—C coupling and improved FEC_{2+}.

In-situ/operando characterization techniques provide the real-time characterization of catalysts in electrocatalytic reduction processes, but are still in their early stages and do not yet allow for observation of the subtle changes that occur in catalysts and intermediates during electrocatalytic reduction. More advanced method needs to be developed to probe the synergistic effects of bimetallic catalysts in CO_2RR.

5 Applications of bimetallic electrocatalysts for CO_2 reduction

CO_2RR involves a complex multi-step electron-mass transfer process with slow electron transfer kinetics. CO and HCOOH are the most common ones due to lower energy requirements and the $2e^-$ transfer process[67]. However, the side-reaction of HER with lower energy requirement also affects the performance of electrocatalytic CO_2RR. Bimetallic catalysts can modify the linear relationship of intermediates and enable multi-step electron transfer to obtain C_{2+} products. Therefore, it is essential to develop catalysts with high selectivity and HER inhibition. Ni and Cu SACs have excellent HER inhibition ability and can combine with other metals to improve catalytic activity through the synergistic effect[44], the outcomes of CO_2RR activated by different bimetallic catalysts is discussed below.

5.1 Generation of carbon monoxide (CO)

CO is a common product of CO_2RR and its reaction pathway is illustrated in Fig. 8a. The oxygen atoms in CO_2 adsorb onto the active sites and undergo a proton-coupled electron transfer (PCET) reaction to form an oxygen-binding intermediate (*COOH), which is subsequently reduced to *CO and then desorbed to form CO[68]. Rashid Iqbal et al.[69] developed MOF-Ni-Fe for CO_2RR, which exhibited higher CO selectivity and excellent stability compared to that of MOF-Ni and MOF-Fe (Fig. 9a). The MOF Ni-Fe had a lower Tafel slope (Fig. 9b) and a smaller radius of the semicircle in the electrochemical impedance spectroscopy (EIS) (Fig. 9c), indicating that the catalyst had faster electron transfer and reaction kinetics in CO_2RR due to the synergistic effect between Ni and Fe. Experimental and computational simulations demonstrated that HER was suppressed at the Fe and Ni sites, and the improved performance was attributed to the synergistic effect between the bimetallic Ni and Fe. However, the generation of H_2 during CO_2RR is inevitable, and additional purification of the product would significantly increase the cost, hindering industrial production[70]. Therefore, stable CO_2 adsorption and reasonable adsorption capacity of *CO intermediates are crucial for optimizing reaction efficiency. Hao et al.[71] proposed the synthesis of Au_1Ni_1/carbon nanofibers (CNFs) by electrospinning to facilitate the conversion of CO_2 to CO. The carbon nanofibers formed after polyvinyl pyrrolidone (PVP) carbonization could restrict the growth of metal nanoclusters and prevent phase separation. The aberration-corrected high-angle annular dark field scanning transmission electron microscopy (AC-HAADF-STEM) image of Au_1Ni_1/CNFs showed lattice fringes of the (111) plane of the AuNi solid-solution alloy. The energy dispersive X-ray spectroscopy (EDX) elemental mapping images demonstrated the uniform distribution of Au and Ni elements within the carbon nanofibers, confirming the formation of AuNi solid-solution alloy nanoparticles in CNFs (Fig. 9(d, e)). In comparison to Au/CNFs and Ni/CNFs, Au_1Ni_1/CNF exhibited a significant improvement in FE_{CO} (Fig. 9f).

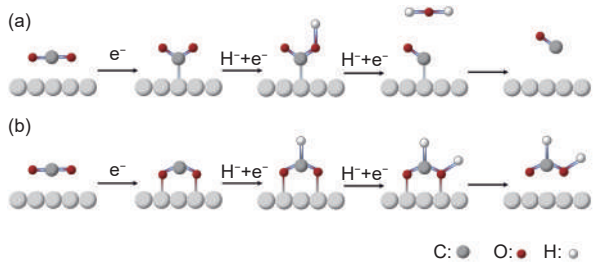

Fig. 8 (a) The pathway diagram for the reduction of CO_2 to CO. (b) The pathway diagram for the reduction of CO_2 to HCOOH

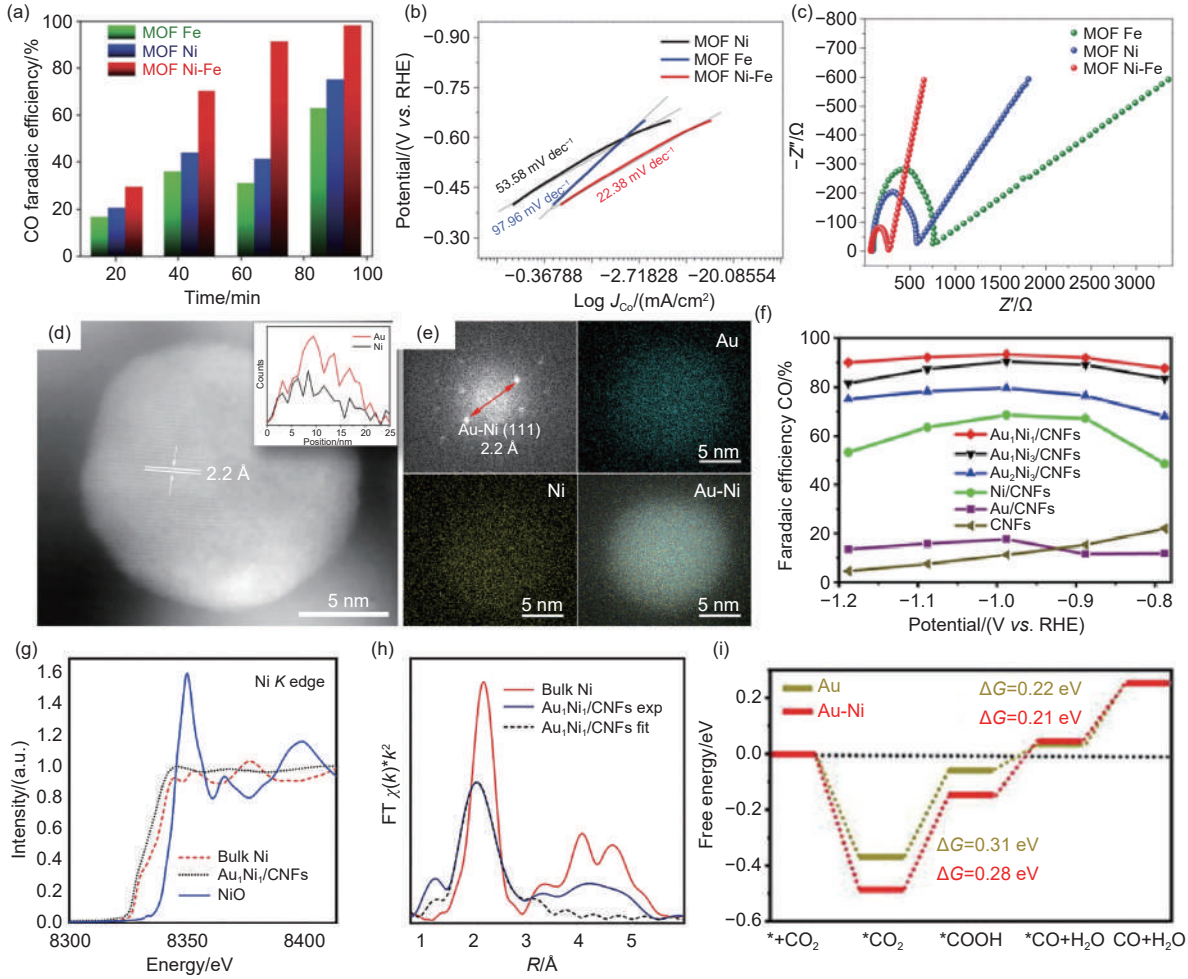

Fig. 9　(a) The FE_{CO} at a fixed potential, (b) Tafel plots, and (c) Electrochemical impedance spectra (EIS) of MOF Ni-Fe, MOF-Ni and MOF-Fe. Reproduced by permission of John Wiley & Sons[69]. (d) AC-HAADF-STEM image of Au_1Ni_1/CNFs. Reproduced by permission of Elsevier[71]. (e) The corresponding fast Fourier transform (FFT) pattern and STEM-EDX elemental mapping images of Au_1Ni_1 NPs including the Au, Ni and the mixed Au and Ni elements. Reproduced by permission of Elsevier[71]. (f) The FE_{CO} for Au/CNFs, Ni/CNFs and AuNi/CNFs. Reproduced by permission of Elsevier[71]. (g) Normalized XANES spectra at the Ni *K*-edge of the Au_1Ni_1/CNFs with compared to Ni and NiO reference. Reproduced by permission of Elsevier[71]. (h) k^3-weighted Fourier transform EXAFS spectra in the R space of Au_1Ni_1/CNFs in comparison to Ni reference. Reproduced by permission of Elsevier[71]. (i) Free energy diagrams for CO_2RR pathways on Au (111) and AuNi (111) model catalyst surface. Reproduced by permission of Elsevier[71]

Synchrotron radiation XAFS confirmed the coordination between Au and Ni, and the introduction of positively charged Ni altered the local electronic structure of the AuNi homogeneous solid-solution alloy (Fig. 9g, h). Operando Raman spectroscopy demonstrated that the change in electronic structure promoted the activation of CO_2 to *COOH and enhanced the adsorption of *COOH on AuNi (111), thus CO selectivity was improved. Theoretical calculations confirmed that the doping of Ni on Au promoted the adsorption of CO_2 molecules on the catalyst surface and facilitated the desorption of *CO intermediates, in agreement with the experimental results (Fig. 9i). This indicates that the synergistic effect of the bimetallic catalyst enhances the CO_2RR activity. At present, the selectivity performance for CO production is close to 100%, but the long-term stability still needs to be improved to meet the standards required for industrial applications.

5.2　Generation of formic acid (HCOOH)

HCOOH is considered to be one of the most economically viable products of CO_2RR due to its high volumetric hydrogen density and relatively convenient transportation[72,73]. It involves a $2e^-$ transfer process, similar to the reduction of CO_2 to CO, but follows a different pathway for HCOOH[74]. It begins

with the adsorption of the CO_2 to the active site by the C atom and is followed by a PCET reaction to produce a carbon-binding intermediate (*OCHO), which is then reduced to HCOOH as the final product (Fig. 8b)[68]. Sn, In and Pb-based catalysts are widely used for the conversion of CO_2 to $HCOO^-$[75]. For example, Li et al.[76] prepared a Cu_xSn_y (x, y is the molar ratio) bimetallic alloy by co-electrodeposition method. As shown in Fig. 10a, b, the FE of H_2 of the Sn CC catalyst at −0.8 V *vs*. RHE was less than 20%, and the FE of HCOOH was about 70%, indicating that the metal Sn strongly suppressed HER. However, the excellent CO_2RR catalytic activity of Sn-based catalysts only occurred at high potential. The FE of the Cu/Sn bimetallic catalyst in the range of from −0.65 to −1.00 V *vs*. RHE was more prominent, indicating that the synergistic effect of Cu and Sn was more helpful for the conversion of CO_2 to HCOOH and reduced the onset potential of the reaction. In addition, the FE_{HCOOH} can be changed by coordinating the bimetal ratio. Wei et al.[77] studied the relationship between the molar ratio of bimetallic In_xCu_y nanoparticles (NPs) (x, y is the molar ratio) and the catalytic performance, and found that In/Cu ratio affects the growth direction of the In (101) facet of the electrocatalyst, which can increase the FE_{HCOOH} of the In-based material. As

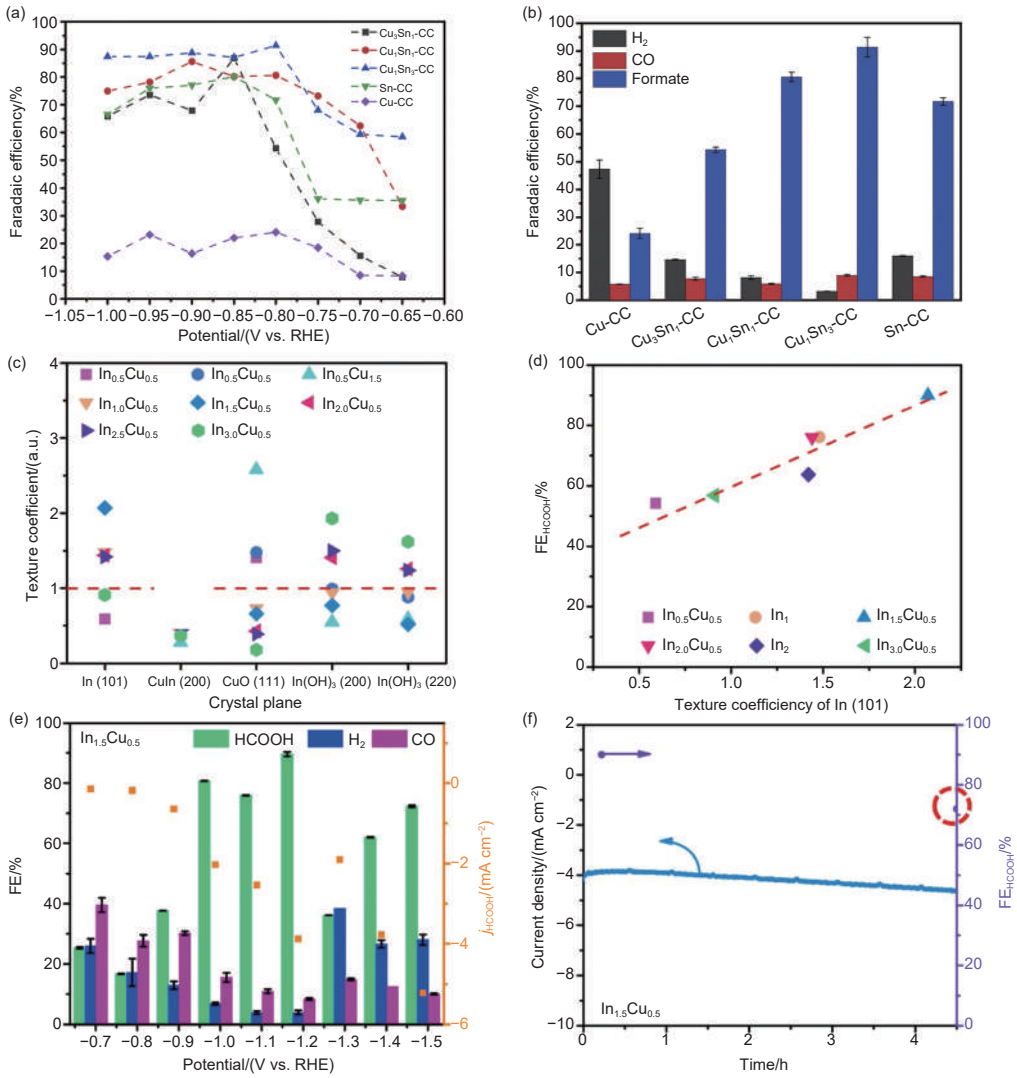

Fig. 10 (a) Faraday efficiencies for CO_2RR on Cn_xSn_y CC catalysts at −0.8 V vs. RHE. Reproduced by permission of Elsevier[76]. (b) Faraday efficiencies for CO_2RR on Cn_xSn_y CC catalysts from −0.65 to −1.00 V vs. RHE. Reproduced by permission of Elsevier[76]. (c) Calculation of texture coefficients based on GIXRD data. Reproduced by permission of Elsevier[77]. (d) Correlation curve between texture coefficients and FE_{HCOOH} in the In (101) plane at −1.2 V *vs*. RHE. Reproduced by permission of Elsevier[77]. (e) The FE for different productions and current density for HCOOH production at selected potentials on $In_{1.5}Cu_{0.5}$ NPs. Reproduced by permission of Elsevier[77]. (f) Stability of $In_{1.5}Cu_{0.5}$ NPs in 0.1 mol L^{-1} $KHCO_3$. Reproduced by permission of Elsevier[77]

shown in Fig. 10c, d, it was found that FE_{HCOOH} was positively correlated with the texture coefficient of the In (101) plane. Therefore, it could be inferred that the In (101) surface of In_xCu_y NPs was beneficial for the reduction of CO_2 to HCOOH. As shown in Fig. 10e, f, the FE_{HCOOH} reached a maximum of 90% at −1.2 V vs. RHE and the FE remained above 70% in the 5 h stability test.

Great strides have been made in the reduction of CO_2 to HCOOH, but it still faces the same issue of poor stability as in the case of CO production. Moreover, the production of HCOOH is often accompanied by the production of CO and H_2, which results in decreased selectivity for HCOOH.

5.3 Generation of other CO_2 reduction products

In addition to CO and HCOOH, CO_2RR can also produce CH_4, CH_3OH and C_{2+} chemicals. However, the reduction of CO_2 to C_1 products, such as CH_4, HCHO and CH_3OH, poses a significant challenge. This is because the reduction process involves multiple hydrogenation steps on *CO, necessitating a greater transfer of electrons, while simultaneously requiring the inhibition of C—C coupling reactions. When the interaction between the active site and CO molecules is weak, it tends to favor CO desorption over the multi-step hydrogenation process[78,79]. The generation of C_{2+} chemicals from CO_2RR is intensively investigated. The process of CO_2RR to C_{2+} involves a complex multi-electron/proton transfer process. When the local concentration of CO intermediates is low, C—C coupling becomes the rate-determining step. At present, various possible routes have been proposed, including *CO—*CO, *CO—*CHO, *CHO—*CHO, *CO—*CH_2, etc[80]. Among them, the formation of bidentate *CO—*CO first requires the stabilization of two *CO intermediates on the active sites, and dimerization occurs at 2 active sites that are near enough. The dimerization reaction is usually considered a key step in the formation of C—C bonds. In addition, some researchers suggest that the PCET accompanies the C—C coupling process. For example, the *CO intermediate forms *CHO or *COH after hydrogenation and undergoes C—C coupling with *CO. Alternatively, the same hydrogenated *CHO or *COH intermediates undergo C—C coupling[81].

Copper-based catalysts or tandem catalysts are widely used to produce C_{2+} chemicals[82]. Copper has a unique C—C coupling capability, but the poor selectivity restricts its further application[83]. Currently, the selectivity of multi-carbon products is improved by modifying the structure[84] or the local reaction environment[85] of the Cu-based catalyst. Alternatively, bimetallic catalysts are synthesized by introducing a second metal to achieve improved selectivity through tandem catalysis. A second metal (such as Au, Ag, or Pd)[66,86,87] with high CO selectivity can generate a large amount of CO, which subsequently spills onto the Cu surface and changes the *CO concentration on the Cu surface. The high *CO concentration on the Cu surface enhances the kinetics of C—C coupling, thus increasing the C_{2+} selectivity[88]. Jia et al.[89] prepared Au—Cu Janus nanocrystals (Au—Cu JNCs) using a seed-mediated growth method, which exhibited excellent C_2 selectivity (Fig. 11a, b). The highest FEC_2 value of the Au-Cu Janus was 46.4%, which was 4.1 times higher than that of the monometallic catalyst Cu nanospheres (NS). The reason for the high C_2 selectivity of Au—Cu Janus was that the conversion of CO_2 to C_2 was split into 2 parts. CO_2 first adsorbed on the Au site to reduce to CO, and then CO overflowed onto the Cu site for C—C coupling (Fig. 11c). At the same time, the distance between the 2 active sites had a non-negligible effect on the catalytic performance. For example, the FEC_2 and C_2 product partial current density of Au—Cu Janus were much higher than those of the Au nanobipyramids (NBP) + Cu NS mixture and the Au NBP@Cu core@shell catalysts (Fig. 11a, b). This phenomenon could be attributed to the intimate integration of Au and Cu domains within Au—Cu JNCs, allowing the two metal active sites to trigger tandem catalysis efficiently and facilitate the conversion of CO_2 to C_2. The Au NBP + Cu NS mixture was simply mixed and lacked the establishment of chemical bonds. As a result, the generated *CO intermediate did not move quickly enough to the Cu active sites for C—C coupling, resulting in a lower FEC_2. Similarly, the Au NBP@Cu core@shell structure achieved close

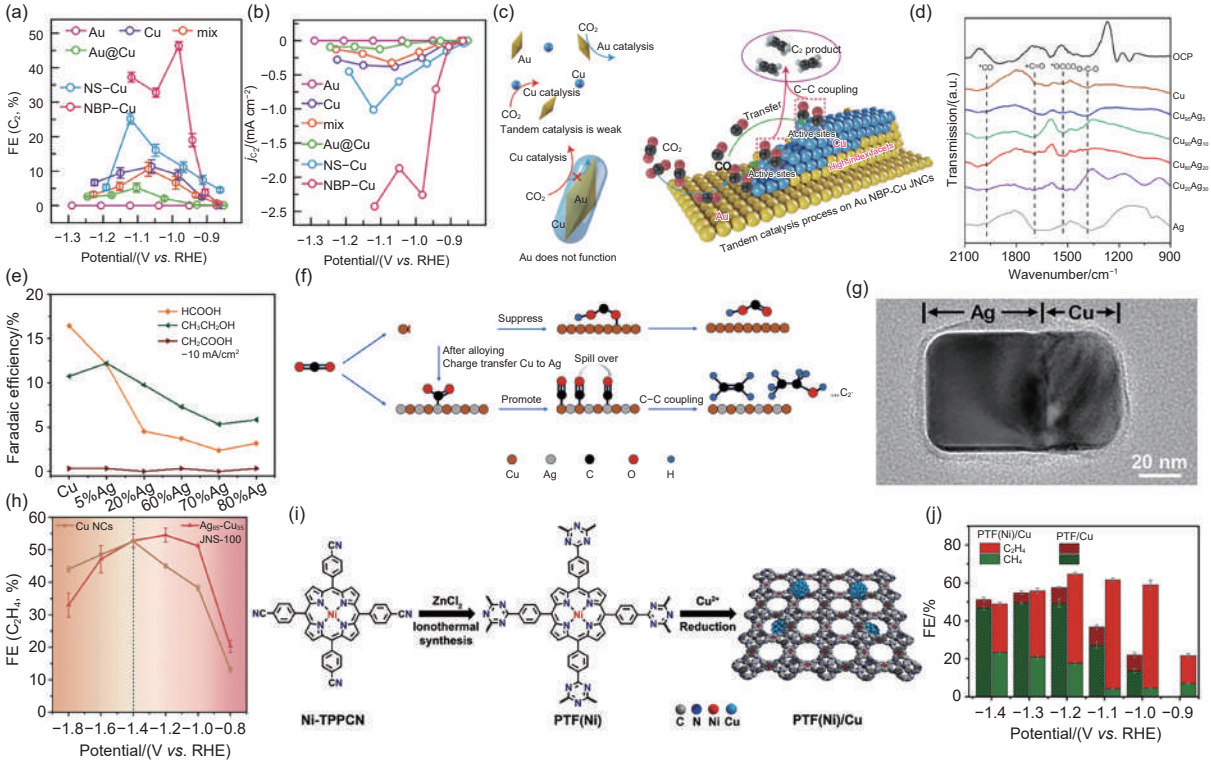

Fig. 11 (a) FEs of C_2 products obtained by using different catalysts. Reproduced by permission of Wiley-VCH[89]. (b) C_2 product partial current density of different catalysts. Reproduced by permission of Wiley-VCH[89]. (c) Catalytic mechanism diagram. Reproduced by permission of Wiley-VCH[89]. (d) Operando SR-FTIR spectroscopy. Reproduced by permission of American Chemical Society[38]. (e) The FE of CO_2RR liquid phase products for different CuAg samples at the total current density of 10 mA/cm^2. Reproduced by permission of American Chemical Society[38]. (f) Proposed reaction mechanisms on Cu and CuAg samples during CO_2RR. Reproduced by permission of American Chemical Society[38]. (g) TEM images of Ag_{65}-Cu_{35} JNS-100. Reproduced by permission of Wiley-VCH[37]. (h) Comparison of FEC_2H_4 between Ag_{65}-Cu_{35} JNS-100 and Cu NCs at different potentials. Reproduced by permission of Wiley-VCH[37]. (i) Fabrication of PTF(Ni)/Cu. Reproduced by permission of John Wiley & Sons[96]. (j) FEs of C_2H_4 and CH_4 at different potentials on PTF(Ni)/Cu and PTF/Cu catalysts. reproduced by permission of John Wiley & Sons[96]

proximity between the Au and Cu domains, but the Au core layer was encapsulated by Cu, reducing the number of CO_2 molecules in contact with the Au sites and consequently reducing the yield of *CO intermediates, which affected the selectivity of the catalyst for C_2. In addition to the influence of the distance between 2 domains on reaction efficiency, the distance between 2 active sites within the same domain is also important for the occurrence of C—C coupling. Bi et al.[90] calculated the catalytic activity and product selectivity of different Cu—Cu atomic distances ($d_{Cu\text{-}Cu}$) by constructing a Cu_2O catalyst model. The calculation results proved that a Cu atom pair with a 2.5 Å increased the *CO adsorption energy and reduced the energy barrier of C—C coupling. Their team prepared ultra-thin 2D $Cu_{2-x}Se$ with abundant Se vacancies, and utilized the generation of Se vacancies to shorten the spatial distance between the surrounding Cu—Cu atoms[91]. Through experiments and density functional theory (DFT) calculations, it was demonstrated that the nearby copper atoms underwent distortion and approach each other due to Se vacancies, resulting in a reduction in the corresponding Cu—Cu spacing from 4.16 to 2.51 Å. The appropriate distance significantly reduced the Gibbs free energy of the asymmetric *CO—*CHO coupling process, thereby improving the selectivity of C_2 products. Xu et al.[38] found that the addition of Ag to the Cu phase inhibited the production of HCOOH during the development of $Cu_{1-x}Ag_x$ (x = 0.05−0.2) alloys. By operando synchrotron radiation Fourier transform infrared spectroscopy (SR-FTIR) analysis, it was observed that the characteristic peak intensity of O—C—O groups decreased after adding a certain amount of Ag (Fig. 11d). This change was consistent with the change in HCOOH production (Fig. 11e).

The O—C—O group is regarded as a key intermediate in the production of HCOOH[92], indicating that Ag entered the Cu phase and inhibited the generation of O—C—O groups, thereby reducing the selectivity of HCOOH. The CO_2RR pathway of $Cu_{1-x}Ag_x$ was proposed in combination with experimental data (Fig. 11f). In the $Cu_{1-x}Ag_x$ alloy, Ag preferred to adsorb C atoms from CO_2 to form M—C bonds and generated large amounts of CO, followed by C—C coupling to form C_{2+}. In addition, the O—C—O group was probably formed by the adsorption of its oxygen atom onto the metal surface to form the M—O bond. Thus, the addition of Ag allowed the CuAg alloy to inhibit the production of HCOOH while facilitating the conversion of CO_2 to C_{2+}.

Crystal plane engineering can effectively control the adsorption and desorption of intermediates involved in the reaction process. Wang et al.[93] enhanced the adsorption of *CO intermediates on the catalyst surface, promoted C—C coupling, and facilitated the desorption of C_2H_4 by adjusting the ratio of (100) and (111) planes in Cu_3N. It has been found that different crystalline facets of metals have different selectivities for CO_2RR. For example, Cu (100) has high selectivity towards C_{2+}[94], while Cu (111) tends to reduce CO_2 to CH_4[95]. Ma et al.[37] synthesized Ag_{65}-Cu_{35} Janus nanostructures (JNS) through the restrictive growth of Cu (100) crystal planes on one of the six faces of Ag nanocubes (Fig. 11g). Compared to pure Cu NCs, Ag_{65}-Cu_{35} JNS demonstrated higher FE for C_2H_4 in the smaller negative potential range (Fig. 11h). This enhanced C_2H_4 selectivity was attributed to the presence of Cu (100) crystal planes and tandem catalysis between the bimetals. On the other hand, developing non-precious metal catalysts also attracted much attention. For instance, the Ni/Cu tandem catalyst was constructed to efficiently convert CO_2 to C_2H_4[96]. Fig. 11i illustrates the uniform growth of Cu nanoparticles (NPs) on the porphyrin triazine backbone containing Ni-N sites (PTF(Ni)). It was evident that the addition of copper in PTF(Ni)/Cu led to the high FEC_2H_4 with 57.3% (Fig. 11j), which was significantly higher than that of PTF/Cu, indicating that the synergistic effect of the bimetal improved the selectivity of C_2H_4. The *operando* ATR-FTIR spectrum of PTF(Ni)/Cu showed a chemisorption peak of CO (*CO), indicating the presence of a large number of *CO intermediates on its surface. Additionally, C—H bonds such as *CHO and *CHCHO, which are key intermediates required for the conversion of CO_2 to C_2H_4, were also observed but were not observed on PTF/Cu. DFT calculations also demonstrated that the enhanced catalytic performance of the bimetal catalyst was due to tandem catalysis between the Ni and Cu bimetals.

Copper-based catalysts can convert CO_2 into various products, including some valuable C_{2+} products. However, the selectivity of single metal copper-based catalysts is low, and the addition of a second metal overcomes this drawback. The synergistic effect of the bimetals can change the adsorption energy of intermediates, improving the selectivity towards C_{2+} products. Despite some achievements made in the production of C_{2+}, the selectivity remains relatively low and stability poor. The amalgamation of bimetallic catalysts with crystal plane engineering, defect engineering, and distance design helps adjust the electronic structure of active sites, promote C—C coupling and facilitate the formation of multi-carbon products. Particularly, the concept of distance design involves studying the influence of distance on the charge distribution of atoms, which affects the adsorption and desorption of intermediates. This can be instrumental in exploring the relationship between catalyst atomic structure and catalytic performance in depth. Currently some major obstacles mar the C_{2+} research. Moreover, the ultimate limit of CO_2RR products is not yet clear. This calls for more research input in this area.

6 Conclusions

Researchers have successfully synthesized a series of bimetallic catalysts capable of converting CO_2 into valuable hydrocarbons and oxygen-containing compounds with remarkable catalytic activity and selectivity under laboratory conditions. Nevertheless,

several significant challenges still need to be addressed:

(1) Given that the CO_2 reduction process involves multiple electron transfer steps, the slow reduction kinetics continue to pose a primary challenge, resulting in reduced catalytic efficiency. Although the synergistic effects of bimetallic materials can result in high FE (FE>90%) for CO or formate, obtaining higher-value products with equivalent FE remains a formidable task. On the other hand, since variations in catalysts and reaction conditions may yield multiple products, researchers are faced with a challenge to precisely control the exclusive formation of a specific product.

(2) Catalysts with clear active sites are crucial for studying catalytic mechanisms. Despite various methods available for synthesizing bimetallic catalysts, it remains difficult to obtain catalysts with precisely located active sites. Synthetic methods that do allow this precise atomic positioning typically have low repeatability. Therefore, there is an urgent need to develop a synthesis process that can obtain active sites with precision while ensuring that the process is facile, in order to further explore the synergistic effects between bimetallic components.

(3) In the CO_2RR process, various reaction intermediates are involved, and the true reaction pathway remains unclear. Furthermore, the catalyst undergoes dynamic changes during the catalytic process, which increases the challenge of identifying the sites that genuinely contribute to catalysis. Therefore, further research employing more robust in-situ characterization techniques is essential to fulfill the requirement for a deeper understanding of the catalyst's structure.

The above challenges collectively impede the industrialization of catalysts, and these issues can be tackled one by one through continuous research and summarization. But, it is likely that additional challenges will be encountered in the future. More efficient methods should be discovered to synthesize efficient catalysts for producing more complex and valuable products. More works are focused on the design of bimetallic catalysts, but further development of advanced characterization techniques should also be emphasized to deeply explore the intrinsic mechanisms of CO_2RR processes in practice. This includes exploring the relationship between the solubility of CO_2 and the reaction efficiency, as well as investigating the impact of CO_2 diffusion and product removal during CO_2RR.

References

[1] Wang Y, Tang Z, Shen S, et al. The influence of heteroatom doping on the performance of carbon-based electrocatalysts for oxygen evolution reactions[J]. New Carbon Materials, 2022, 37(2): 321-336.

[2] Wang H, Zhao Y, Yang Z, et al. Oxygen-incorporated carbon nitride porous nanosheets for highly efficient photoelectrocatalytic CO_2 reduction to formate[J]. New Carbon Materials, 2022, 37(6): 1135-1142.

[3] Qu T, Hu J, Dai X, et al. Electrospinning highly dispersed Ru nanoparticle-embedded carbon nanofibers boost CO_2 reduction in a H_2/CO_2 fuel cell[J]. ACS Applied Materials & Interfaces, 2021, 13(20): 23523-23531.

[4] Ren M, Guo X and Huang S. Coordination-tuned Fe single-atom catalyst for efficient CO_2 electroreduction: The power of B atom[J]. Chemical Engineering Journal, 2022, 433: 134270.

[5] Lai W, Ma Z, Zhang J, et al. Dynamic evolution of active sites in electrocatalytic CO_2 reduction reaction: Fundamental understanding and recent progress[J]. Advanced Functional Materials, 2022, 32(16): 2111193.

[6] Dai S, Huang T, Liu W, et al. Enhanced CO_2 electrochemical reduction performance over Cu@AuCu catalysts at high noble metal utilization efficiency[J]. Nano Letters, 2021, 21(21): 9293-9300.

[7] Zhi W, Liu Y, Shan S, et al. Efficient electroreduction of CO_2 to C_2-C_3 products on Cu/Cu_2O@N-doped graphene[J]. Journal of CO_2 Utilization, 2021, 50: 101594.

[8] Xiong L, Zhang X, Chen L, et al. Geometric modulation of local CO flux in Ag@Cu_2O nanoreactors for steering the CO_2RR pathway toward high-efficacy methane production[J]. Advanced Materials, 2021, 33(32): e2101741.

[9] Beheshti M, Kakooei S, Ismail M C, et al. Investigation of CO_2 electrochemical reduction to syngas on Zn/Ni-based electrocatalysts using the cyclic voltammetry method[J]. Electrochimica Acta, 2020, 341: 135976.

[10] Wei B, Hao J, Ge B, et al. Highly efficient electrochemical carbon dioxide reduction to syngas with tunable ratios over pyridinic-nitrogen rich ultrathin carbon nanosheets[J]. Journal of Colloid and Interface Science, 2022, 608: 2650-2659.

[11] Nie W and McCrory C C L. Strategies for breaking molecular scaling relationships for the electrochemical CO_2 reduction reaction[J]. Dalton Transactions, 2022, 51(18): 6993-7010.

[12] Cao Z, Liu S, Xu K, et al. Predictable interfacial mass transfer intensification of Sn–N doped multichannel hollow carbon nanofibers for the CO_2 electro-reduction reaction[J]. Sustainable Energy & Fuels, 2021, 5(12): 3097-3101.

[13] Wei X, Xiao S, Wu R, et al. Activating COOH* intermediate by

$Ni/Ni_3ZnC_{0.7}$ heterostructure in porous N-doped carbon nanofibers for boosting CO_2 electroreduction[J]. Applied Catalysis B: Environmental, 2022, 302: 120861.

[14] Bagchi D, Sarkar S, Singh A K, et al. Potential- and time-dependent dynamic nature of an oxide-derived PdIn nanocatalyst during electrochemical CO_2 reduction[J]. ACS Nano, 2022, 16(4): 6185-6196.

[15] Zhao Z and Lu G. Circumventing the scaling relationship on bimetallic monolayer electrocatalysts for selective CO_2 reduction[J]. Chemical Science, 2022, 13(13): 3880-3887.

[16] Zhang W, Zeng J, Liu H, et al. Co_xNi_{1-x} nanoalloys on N-doped carbon nanofibers: Electronic regulation toward efficient electrochemical CO_2 reduction[J]. Journal of Catalysis, 2019, 372: 277-286.

[17] Huang J E, Li F, Adnan O, et al. CO_2 electrolysis to multicarbon products in strong acid[J]. Science, 2021, 372(6546): 1074-1078.

[18] Zou J, Lee C Y and Wallace G G. Boosting formate production from CO_2 at high current densities over a wide electrochemical potential window on a SnS catalyst[J]. Advanced Science, 2021, 8(15): e2004521.

[19] An B, Zhou J, Zhu Z, et al. Uncovering the coordination effect on the Ni single-atom catalysts for CO_2 reduction including vacancy defect and non-vacancy defect structures[J]. Fuel, 2022, 310: 122472.

[20] Cheng H, Wu X, Li X, et al. Construction of atomically dispersed $Cu-N_4$ sites via engineered coordination environment for high-efficient CO_2 electroreduction[J]. Chemical Engineering Journal, 2021, 407: 126842.

[21] Kumar A, Vashistha V K, Das D K, et al. M-N-C-based single-atom catalysts for H_2, O_2 & CO_2 electrocatalysis: Activity descriptors, active sites identification, challenges and prospects[J]. Fuel, 2021, 304: 121420.

[22] Yang H, Wang X, Wang S, et al. Double boosting single atom $Fe-N_4$ sites for high efficiency O_2 and CO_2 electroreduction[J]. Carbon, 2021, 182: 109-116.

[23] Jia Y, Li F, Fan K, et al. Cu-based bimetallic electrocatalysts for CO_2 reduction[J]. Advanced Powder Materials, 2022, 1(1): 100012.

[24] Ouyang Y, Shi L, Bai X, et al. Breaking scaling relations for efficient CO_2 electrochemical reduction through dual-atom catalysts[J]. Chemical Science, 2020, 11(7): 1807-1813.

[25] Wei X, Wei S, Cao S, et al. Cu acting as Fe activity promoter in dual-atom Cu/Fe-NC catalyst in CO_2RR to C1 products[J]. Applied Surface Science, 2021, 564: 150423.

[26] Gao Y, Xiao H, Ma X, et al. Gallium-indium bimetal sites in the indium-gallium metal organic framework for efficient electrocatalytic reduction of carbon dioxide into formate[J]. Journal of Materials Chemistry A, 2024.

[27] Hu J, Yang F, Qu J, et al. Synergetic bimetallic catalysts: a remarkable platform for efficient conversion of CO_2 to high value-added chemicals[J]. Journal of Energy Chemistry, 2023, 87: 162-191.

[28] Chen Y, Li X Y, Chen Z, et al. Efficient multicarbon formation in acidic CO_2 reduction via tandem electrocatalysis[J]. Nature Nanotechnology, 2024, 19(3): 311-318.

[29] Zhang B A and Nocera D G. Cascade electrochemical reduction of carbon dioxide with bimetallic nanowire and foam electrodes[J]. ChemElectroChem, 2021, 8(10): 1918-1924.

[30] Zhang W, Chao Y, Zhang W, et al. Emerging dual-atomic-site catalysts for efficient energy catalysis[J]. Advanced Materials, 2021, 33(36): e2102576.

[31] Wang Y, Park B J, Paidi V K, et al. Precisely constructing orbital coupling-modulated dual-atom Fe pair sites for synergistic CO_2 electroreduction[J]. ACS Energy Letters, 2022, 7(2): 640-649.

[32] Wang F, Xie H, Liu T, et al. Highly dispersed CuFe-nitrogen active sites electrode for synergistic electrochemical CO_2 reduction at low overpotential[J]. Applied Energy, 2020, 269: 115029.

[33] Liu K, Li J, Liu Y, et al. Dual metal atom catalysts: Advantages in electrocatalytic reactions[J]. Journal of Energy Chemistry, 2023, 79: 515-534.

[34] Guo Z, Zhu H, Yang G, et al. Synergistic engineering of heteronuclear Ni-Ag dual-atom catalysts for high-efficiency CO_2 electroreduction with nearly 100% CO selectivity[J]. Chemical Engineering Journal, 2023, 476: 146556.

[35] Leverett J, Daiyan R, Gong L, et al. Designing undercoordinated $Ni-N_x$ and $Fe-N_x$ on holey graphene for electrochemical CO_2 conversion to syngas[J]. ACS Nano, 2021, 15(7): 12006-12018.

[36] Yang R, Duan J, Dong P, et al. In situ halogen-ion leaching regulates multiple sites on tandem catalysts for efficient CO_2 electroreduction to C_{2+} products[J]. Angewandte Chemie International Edition, 2022, 61(21): e202116706.

[37] Ma Y, Yu J, Sun M, et al. Confined growth of silver-copper janus nanostructures with (100) facets for highly selective tandem electrocatalytic carbon dioxide reduction[J]. Advanced Materials, 2022, 34(19): e2110607.

[38] Xu Y, Li C, Xiao Y, et al. Tuning the selectivity of liquid products of CO_2RR by Cu-Ag alloying[J]. ACS Applied Materials & Interfaces, 2022, 14(9): 11567-11574.

[39] Wang J, Cheng C, Huang B, et al. Grain-boundary-engineered La_2CuO_4 perovskite nanobamboos for efficient CO_2 reduction reaction[J]. Nano Letters, 2021, 21(2): 980-987.

[40] Zhang S, Zhao S, Qu D, et al. Electrochemical reduction of CO_2 toward C_2 valuables on Cu@Ag core-shell tandem catalyst with tunable shell thickness[J]. Small, 2021, 17(37): e2102293.

[41] Yang Z, Wang H, Bi X, et al. Bimetallic In_2O_3/Bi_2O_3 catalysts enable highly selective CO_2 electroreduction to formate within ultra-broad potential windows[J]. Energy & Environmental Materials, 2023, 7: e12508.

[42] Ying Y, Luo X, Qiao J, et al. "More is different: " Synergistic effect and structural engineering in double-atom catalysts[J]. Advanced Functional Materials, 2020, 31(3): 2007423.

[43] Ji S, Chen Y, Wang X, et al. Chemical synthesis of single atomic site catalysts[J]. Chemical Reviews, 2020, 120(21): 11900-11955.

[44] Cheng H, Wu X, Feng M, et al. Atomically dispersed Ni/Cu dual sites for boosting the CO_2 reduction reaction[J]. ACS Catalysis, 2021, 11(20): 12673-12681.

[45] Ren W, Tan X, Yang W, et al. Isolated diatomic Ni-Fe metal-nitrogen sites for synergistic electroreduction of CO_2[J]. Angewandte Chemie International Edition, 2019, 58(21): 6972-6976.

[46] Zhang Y, Li P, Zhao C, et al. Multicarbons generation factory: CuO/Ni single atoms tandem catalyst for boosting the productivity of CO_2 electrocatalysis[J]. Science Bulletin, 2022, 67(16): 1679-1687.

[47] Zhao D, Zhuang Z, Cao X, et al. Atomic site electrocatalysts for water splitting, oxygen reduction and selective oxidation[J]. Chemical Society Reviews, 2020, 49(7): 2215-2264.

[48] Gong Q, Wang Y, Ren X, et al. Ultra-low-loaded Ni-Fe dimer anchored to nitrogen/oxygen sites for boosting electroreduction of carbon dioxide[J]. ChemSusChem, 2021, 14(20): 4499-4506.

[49] Zhang Z, Wen G, Luo D, et al. "Two ships in a bottle" design for Zn-Ag-O catalyst enabling selective and long-lasting CO_2 electroreduction[J]. Journal of the American Chemical Society, 2021, 143(18): 6855-6864.

[50] Zeng J, Bejtka K, Ju W, et al. Advanced Cu-Sn foam for selectively converting CO_2 to CO in aqueous solution[J]. Applied Catalysis B: Environmental, 2018, 236: 475-482.

[51] Rahaman M, Kiran K, Zelocualtecatl Montiel I, et al. Suppression of the hydrogen evolution reaction is the key: Selective electrosynthesis of formate from CO_2 over porous $In_{55}Cu_{45}$ catalysts[J]. ACS Applied Materials & Interfaces, 2021, 13(30): 35677-35688.

[52] Nellist P D and Pennycook S J. Incoherent imaging using dynamically scattered coherent electrons[J]. Ultramicroscopy, 1998, 78(1-4): 111-124.

[53] Loos J J, Sourty E E, Lu K K, et al. Imaging polymer systems with high-angle annular dark field scanning transmission electron microscopy (HAADF-STEM)[J]. Macromolecules, 2009, 42(7): 2581-2586.

[54] Zhang N, Zhang X, Kang Y, et al. A supported Pd_2 dual-atom site Catalyst for efficient electrochemical CO_2 reduction[J]. Angewandte Chemie International Edition, 2021, 60(24): 13388-13393.

[55] Li Y, Chen C, Cao R, et al. Dual-atom Ag_2/graphene catalyst for efficient electroreduction of CO_2 to CO[J]. Applied Catalysis B: Environmental, 2020, 268: 118747.

[56] Groot F M F d. Site-selective XAFS: A new tool for catalysis research[J]. Topics in Catalysis, 2020, 10(3-4): 179-186.

[57] Oversteeg C H M v, Doan H Q, Groot F M F d, et al. In situ X-ray absorption spectroscopy of transition metal based water oxidation catalysts[J]. Chemical Society Reviews, 2017, 46(1): 102-125.

[58] Zhao S, Yang Y and Tang Z. Insight into structural evolution, active sites, and stability of heterogeneous electrocatalysts[J]. Angewandte Chemie International Edition, 2022, 61(11): e202110186.

[59] Luo Z, Yin Z, Yu J, et al. General synthetic strategy to ordered mesoporous carbon catalysts with single-atom metal sites for electrochemical CO_2 reduction[J]. Small, 2022, 18(16): e2107799.

[60] Koide A, Fujikawa T and Ichikuni N. Recent progress in EXAFS/NEXAFS spectroscopy[J]. Journal of Electron Spectroscopy and Related Phenomena, 2014, 195: 375-381.

[61] Lytle F W. The EXAFS family tree: A personal history of the development of extended X-ray absorption fine structure[J]. Journal of Synchrotron Radiation, 1999, 6: 123-134.

[62] Frenkel A I. Applications of extended X-ray absorption fine-structure spectroscopy to studies of bimetallic nanoparticle catalysts[J]. Chemical Society Reviews, 2012, 41(24): 8163-8178.

[63] Yang X, Wang M, Zachman M J, et al. Binary atomically dispersed metal-site catalysts with core-shell nanostructures for O_2 and CO_2 reduction reactions[J]. Small Science, 2021, 1(10): 2100046.

[64] Hu F, Yang L, Jiang Y, et al. Ultrastable Cu catalyst for CO_2 electroreduction to multicarbon liquid fuels by tuning C-C coupling with CuTi subsurface[J]. Angewandte Chemie International Edition, 2021, 60(50): 26122-26127.

[65] Rahaman M, Kiran K, Montiel I Z, et al. Selective n-propanol formation from CO_2 over degradation-resistant activated PdCu alloy foam electrocatalysts[J]. Green Chemistry, 2020, 22(19): 6497-6509.

[66] Zheng Y, Zhang J, Ma Z, et al. Seeded growth of gold-copper janus nanostructures as a tandem catalyst for efficient electroreduction of CO_2 to C_{2+} products[J]. Small, 2022, 18(19): e2201695.

[67] Liu W, Wang K, Gong L, et al. Edge-located Fe-N_4 sites on porous graphene-like nanosheets for boosting CO_2 electroreduction[J]. Chemical Engineering Journal, 2022, 431: 134269.

[68] Liu C, Mei X, Han C, et al. Tuning strategies and structure effects of electrocatalysts for carbon dioxide reduction reaction[J]. Chinese Journal of Catalysis, 2022, 43(7): 1618-1633.

[69] Iqbal R, Akbar M B, Ahmad A, et al. Exploring the synergistic effect of novel Ni-Fe in 2D bimetallic metal-organic frameworks for enhanced electrochemical reduction of CO_2[J]. Advanced Materials Interfaces, 2021, 9(1): 2101505.

[70] Zhang H, Wang H, Jia S, et al. CoN_4 active sites in a graphene matrix for the highly efficient electrocatalysis of CO_2 reduction[J]. New Carbon Materials, 2022, 37(4): 734-742.

[71] Hao J, Zhu H, Li Y, et al. Tuning the electronic structure of AuNi homogeneous solid-solution alloy with positively charged Ni center for highly selective electrochemical CO_2 reduction[J]. Chemical Engineering Journal, 2021, 404: 126523.

[72] Jouny M, Luc W and Jiao F. General techno-economic analysis of CO_2 electrolysis systems[J]. Industrial & Engineering Chemistry Research, 2018, 57(6): 2165-2177.

[73] Yang Zhongxue, Wang Hongzhi, Fei Xiang, et al. MOF derived bimetallic CuBi catalysts with ultra-wide potential window for high-efficient electrochemical reduction of CO_2 to formate[J]. Applied Catalysis B: Environmental 2021, 298 120571.

[74] Li W, Yu C, Tan X, et al. Recent advances in the electroreduction of carbon dioxide to formic acid over carbon-based materials[J]. New Carbon Materials, 2022, 37(2): 277-287.

[75] Chen C, Sun M, Wang K, et al. Dual-metal single-atomic catalyst: The challenge in synthesis, characterization, and mechanistic investigation for electrocatalysis[J]. SmartMat, 2022, 3(4): 533-564.

[76] Li H, Yue X, Qiu Y, et al. Selective electroreduction of CO_2 to formate over the co-electrodeposited Cu/Sn bimetallic catalyst[J]. Materials Today Energy, 2021, 21: 100797.

[77] Wei B, Xiong Y, Zhang Z, et al. Efficient electrocatalytic reduction of CO_2 to HCOOH by bimetallic In-Cu nanoparticles with controlled growth facet[J]. Applied Catalysis B: Environmental, 2021, 283: 119646.

[78] Liu Y, Zhu H, Zhao Z, et al. Insight into the effect of the d-orbital energy of copper ions in metal –organic frameworks on the selectivity of electroreduction of CO_2 to CH_4[J]. ACS Catalysis, 2022, 12(5): 2749-2755.

[79] Wu Y, Jiang Z, Lu X, et al. Domino electroreduction of CO_2 to methanol on a molecular catalyst[J]. Nature, 2019, 575(7784): 639-642.

[80] Farooqi S A, Farooqi A S, Sajjad S, et al. Electrochemical reduction of carbon dioxide into valuable chemicals: a review[J].

Environmental Chemistry Letters, 2023, 21(3): 1515-1553.

[81] Liu S, Zhang B, Zhang L, et al. Rational design strategies of Cu-based electrocatalysts for CO_2 electroreduction to C_2 products[J]. Journal of Energy Chemistry, 2022, 71: 63-82.

[82] Dutta A, Montiel I Z, Erni R, et al. Activation of bimetallic AgCu foam electrocatalysts for ethanol formation from CO_2 by selective Cu oxidation/reduction[J]. Nano Energy, 2020, 68: 104331.

[83] Wang W, Ma Z, Fei X, et al. Joint tuning the morphology and oxygen vacancy of Cu_2O by ionic liquid enables high-efficient CO_2 reduction to C_2 products[J]. Chemical Engineering Journal, 2022, 436: 135029.

[84] Pan Y, Li H, Xiong J, et al. Protecting the state of Cu clusters and nanoconfinement engineering over hollow mesoporous carbon spheres for electrocatalytical C-C coupling[J]. Applied Catalysis B: Environmental, 2022, 306: 121111.

[85] Pham T H M, Zhang J, Li M, et al. Enhanced electrocatalytic CO_2 reduction to C_{2+} products by adjusting the local reaction environment with polymer binders[J]. Advanced Energy Materials, 2022, 12(9): 2103663.

[86] Choukroun D, Pacquets L, Li C, et al. Mapping composition-selectivity relationships of supported sub-10 nm Cu-Ag nanocrystals for high-rate CO_2 electroreduction[J]. ACS Nano, 2021, 15(9): 14858-14872.

[87] Mosali V S S, Li L, Puxty G, et al. Ultra-thin Pd and CuPd bimetallic alloy nanosheets for electrochemical reduction of CO_2[J]. ChemElectroChem, 2022, 9(5): e202101227.

[88] Zhang X, Liu C, Zhao Y, et al. Atomic nickel cluster decorated defect-rich copper for enhanced C_2 product selectivity in electrocatalytic CO_2 reduction[J]. Applied Catalysis B: Environmental, 2021, 291: 120030.

[89] Jia H, Yang Y, Chow T H, et al. Symmetry-broken Au-Cu heterostructures and their tandem catalysis process in electrochemical CO_2 reduction[J]. Advanced Functional Materials, 2021, 31(27): 2101255.

[90] Bi X, Yan Y, Wang H, et al. Electroreduction of CO_2 to C_2H_4 regulated by spacing effect: mechanistic insights from DFT studies[J]. Energy Material Advances, 2023, 4.

[91] Wang H, Bi X, Yan Y, et al. Efficient electrocatalytic reduction of CO_2 to ethanol enhanced by spacing effect of Cu-Cu in $Cu_{2-x}Se$ nanosheets[J]. Advanced Functional Materials, 2023, 33: 2214946.

[92] Firet N J and Smith W A. Probing the reaction mechanism of CO_2 electroreduction over Ag films via operando infrared spectroscopy[J]. ACS Catalysis, 2016, 7(1): 606-612.

[93] Wang H, Bi X, Zhao Y, et al. Cu_3N nanoparticles with both (100) and (111) facets for enhancing the selectivity and activity of CO_2 electroreduction to ethylene[J]. New Journal of Chemistry, 2022, 46(26): 12523-12529.

[94] Calle Vallejo F and Koper M T. Theoretical considerations on the electroreduction of CO to C_2 species on Cu(100) electrodes[J]. Angewandte Chemie International Edition, 2013, 52(28): 7282-5.

[95] Schouten K J P, Gallent E P and Koper M T M. Structure sensitivity of the electrochemical reduction of carbon monoxide on copper single crystals[J]. ACS Catalysis, 2013, 3(6): 1292-1295.

[96] Meng D, Zhang M, Si D, et al. Highly selective tandem electroreduction of CO_2 to ethylene over atomically isolated nickel-nitrogen site/copper nanoparticle catalysts[J]. Angewandte Chemie International Edition, 2021, 60(48): 25485-25492.

)